

Gravity Modeling for High-Accuracy GPS/INS Integration

Dorota A. Grejner-Brzezinska and Jin Wang

The Ohio State University Center for Mapping,

Columbus, OH

ABSTRACT

The feasibility of improving airborne GPS/INS integrated navigation by use of accurate deflection of the vertical (DOV) information is investigated in this paper. Based on the available 2'×2' DOV grid, tests were run on GPS/INS navigation data, and the results were compared with the corresponding results where the DOV compensation was not used. The issue of stochastic modeling of the anomalous gravity field in the state vector of the integrated filter is also addressed here. The tests were conducted using the Airborne Integrated Mapping System (AIMS™), whose positioning component is based on a tightly integrated GPS/INS. The system is designed to provide orientation and position of an aerial platform, with estimated accuracy of 4-7 centimeters in position, and ~ 10 arcsec in orientation in post-mission mode. A brief overview of the system is also given, including a discussion of current error modeling and airborne test results.

INTRODUCTION

Integrated systems based on Global Positioning System (GPS) and Inertial Navigation System (INS) generated increased interest in the airborne survey and remote sensing community over the past few years as a tool for direct georeferencing of aerial imagery [17, 25, 20, 22, 1, 28, 7]. At the same time, the use of GPS/INS systems for airborne gravimetry has been researched by the geodetic and navigation community [16, 3, 26, 6, 12, 13, 10, 31]. With full operational GPS

capability, it has been recognized that an optimal combination of GPS with inertial navigation brings a number of advantages over stand-alone inertial or GPS navigation. GPS contributes its high accuracy and stability over time, enabling continuous monitoring of inertial sensor errors. Implementation of closed-loop INS error calibration allows continuous, on-the-fly error update that bounds INS errors, leading to increased estimation accuracy. On the other hand, INS contributes immunity to GPS outages, continuous attitude solution, and reduction of the GPS ambiguity search volume/time. Using a GPS-calibrated, high to medium accuracy inertial system, attitude accuracy in the range of 10-30 arcsec can be achieved [27, 1, 4, 7, 8]. Conversely, an array of GPS antennas mounted on a mobile platform can also provide attitude estimates, complementary to those, determined by the calibrated gyro observable. The GPS-derived attitude components, available usually at 1-10 Hz rate, can be good to 1-2 arcmin [18, 31], depending mainly on the GPS antenna baseline length and orientation with respect to line-of-sight, and multipath level. The issue of ambiguity resolution is not addressed here; it is assumed that some ambiguity resolution method is applied before the attitude components are estimated. For example, the Ashtech GPS 3DF-ADU multi-antenna system is capable of providing 2-Hz attitude information, with accuracy estimated at 0.2° RMS for heading, and 0.4° RMS for pitch and roll, based a 1-meter square antenna array (3DF-ADU Manual), and the Trimble TANS Vector delivers 10-Hz attitude information with an accuracy of 0.3° for 1-meter baseline (TANS Vector product description). In order to obtain 0.1° pointing accuracy, however, the baselines connecting the electrical centers of GPS antennas must be known to within 2 mm on a 1 m baseline [32]. This requires baseline estimation by the attitude determination filter, as the baseline separation can change from the pre-surveyed value during the airborne or spaceborne mission. In general, the stand-alone multi-antenna GPS provides less accurate, and at

much lower frequency, attitude information as compared to integrated GPS/INS with a high accuracy inertial system supported by differential GPS (DGPS). Using quality DGPS it's possible to bound the gyro drifts and obtain high accuracy attitude estimates even with a single roving GPS antenna. The implementation of a multi-array GPS system, however, may become more important for the integrated systems that utilize low accuracy INS, rendering more robust system. The gyros can estimate the phase differences related to the airborne GPS baselines, forming a class of external updates to the integrated filter. In such a case, special care should be exercised towards proper parameterization and dynamic modeling of the filter states, since attitude and baseline errors (that need to be added to the state vector) are closely coupled, and some observability issues can arise. Moreover, an attitude motion is needed to separate baseline and attitude errors in the combined filter. In addition, since attitude is usually needed with respect to some frame different from the body frame defined by the GPS antennas, a transformation between the frame defined by the GPS antenna array, and the frame of interest is needed. Some external measurement is required to resolve the rotation between these two frames. However, if any baseline flexure is present, this relationship will not be constant, and would require external information to resolve this rotation.

The Ohio State University Center for Mapping has developed an integrated GPS/INS system as a part of a fully digital Airborne Integrated Mapping System (AIMS™), designed for large-scale mapping and other precise mapping applications. The AIMS™ positioning module is based on a tightly integrated, dual frequency differential GPS (single roving antenna) and the Litton LN100 inertial navigation system. The project's goal is to acquire the position and orientation of an aerial platform with an accuracy of 4-7 centimeters and below 10 arcsec, respectively, in

post-processing mode. This level of accuracy offers a possibility to reduce or even eliminate the need for aerotriangulation, translating to substantial savings in data processing time and cost in aerial surveying. The performance of AIMS™ positioning has been repeatedly evaluated during several tests with different flight conditions and varying base-rover separation [9, 29]. The system’s accuracy estimates derived from the covariance matrix were not yet validated by an independent, high-accuracy ground truth test; the major reason for that being the limited accuracy of the aerotriangulation solution, as presented by [29]. However, assuming reliable sensor error modeling [21], the internally estimated position and attitude error terms can be considered as a dependable measure of accuracy. It is our belief that the sensor error models implemented in the integrated filter are reliable (see Table 2), since they are based on several years of testing by the LN100 manufacturer; therefore, the RMS analysis should provide a good indication of system accuracy. Further tests against the ground truth are currently in progress. Table 1 shows the typical errors internally estimated from several test flights [9]. It should be mentioned that carefully planned maneuvers performed between the steady portions of the test flights were able to keep the platform orientation at less than 10 arcsec level even for the long base-rover separation.

Estimated Error Components (RMS)	Base-rover separation				Units
	50	100	200	350	[km]
North coordinate	10	9	9	15	[mm]
East Coordinate	9	8	8	15	[mm]
Vertical Coordinate	20	21	18	31	[mm]
Heading	6.0	6.3	7.5	7.0	[arcsec]

]
Pitch	3.0	3.7	5.1	5.1	[arcsec]
Roll	3.3	4.1	5.1	5.0	[arcsec]

Table 1. Estimated standard deviations in position and orientation as a function of base-rover separation.

This paper presents the ongoing effort to upgrade the system to provide even more accurate estimates of position, and especially, orientation. In the integrated system during the GPS outages, the quality of free-inertial navigation with the high- to medium-accuracy INS currently may well depend on the knowledge of the local gravity field. Therefore, gravity anomaly and deflection maps given on dense grids, based on gravimetric surveys, are becoming more significant to precise navigation. High-accuracy vertical deflection compensation should refine not only the positioning accuracy, but also the attitude determination of the platform. On one hand, the method of improving attitude estimates by accurate vertical deflection information should be labeled as “low altitude technique” due to the rapid attenuation of DOV with altitude. On the other hand, the AIMS™ system is designed particularly for large-scale mapping, and therefore, is naturally confined to low altitudes, where the method is specifically applicable. For the high altitude flights supported by integrated GPS/INS, the multi-antenna array may become an optimal solution, providing attitude determination support independently of the platform’s altitude. In this paper the implementation of the National Imagery and Mapping Agency (NIMA) 2’×2’ deflection of the vertical (DOV) data, and the resulting performance evaluation of the platform position and orientation, are presented.

AIMS™: CURRENT CONFIGURATION

The AIMS™ positioning component currently comprises two dual-frequency, single-antenna Trimble 4000SSI GPS receivers, and a medium-accuracy, and highly reliable, strapdown Litton LN-100 inertial navigation system, based on the Zero-lock™ Laser Gyro (ZLG™) and an A-4 accelerometer triad (0.8 nmi/h CEP, gyro bias – 0.003°/h, accelerometer bias – 25µg). The LN-100 firmware, modified for the AIMS™ project, allows for access to the raw IMU data, updated at 256 Hz [21]. Estimation of errors in position, velocity, and attitude, as well as errors in inertial and GPS measurements, is accomplished by a centralized Kalman filter that processes GPS L1/L2 phase observables in double-differenced mode, together with the INS strapdown navigation solution [4, 7]. The state vector components and their stochastic model representation are presented in Table 2. Figure 1 illustrates the current hardware configuration.

Kalman Filter States¹	Number of States	Initial Conditions (1 sigma)
Navigation Parameters		
Position errors	3	1.0 m
Velocity errors	3	0.5 m/s
Attitude errors	2	0.01°
Heading	1	0.05°
Accelerometer Errors		
Biases	3	30.0µg
Scale factor errors	3	50 ppm, (5.0 µg*√s)
Gyro Errors		
Drifts	3	0.010 deg/h (0.001deg/√h)
Gravity		
Deflection	2	25 mgal

(Gauss-Markov, T = 20 nmi) Anomaly (Gauss-Markov, T = 20 nmi)	1	35 mgal (5mgal) ²
GPS Errors Ionospheric delay (random walk)	Number of DD	2 cm 1 mm* \sqrt{s}

¹ GPS lever arm errors can be included in the filter state vector

² refers to the solution with DOV compensation

Table 2. Filter state vector characteristics.

A compact form of the state equation of the filter model can be presented by the following matrix equation:

$$\begin{bmatrix} \dot{\mathbf{x}}_{Nav} \\ \dot{\mathbf{x}}_{Grav} \\ \dot{\mathbf{x}}_{Acc} \\ \dot{\mathbf{x}}_{Gyro} \\ \dot{\mathbf{x}}_{Ant} \\ \dot{\mathbf{x}}_{GPS} \end{bmatrix} = \begin{bmatrix} F_{11} & F_{12} & F_{13} & F_{14} & 0 & 0 \\ 0 & F_{22} & 0 & 0 & 0 & 0 \\ 0 & 0 & 0 & 0 & 0 & 0 \\ 0 & 0 & 0 & 0 & 0 & 0 \\ 0 & 0 & 0 & 0 & 0 & 0 \\ 0 & 0 & 0 & 0 & 0 & 0 \end{bmatrix} \begin{bmatrix} \mathbf{x}_{Nav} \\ \mathbf{x}_{Grav} \\ \mathbf{x}_{Acc} \\ \mathbf{x}_{Gyro} \\ \mathbf{x}_{Ant} \\ \mathbf{x}_{GPS} \end{bmatrix} + \begin{bmatrix} \mathbf{w}_{Nav} \\ \mathbf{w}_{Grav} \\ \mathbf{w}_{Acc} \\ \mathbf{w}_{Gyro} \\ 0 \\ \mathbf{w}_{GPS} \end{bmatrix} \quad (1)$$

where \mathbf{x}_{Nav} , \mathbf{x}_{Acc} , \mathbf{x}_{Gyro} , \mathbf{x}_{Grav} , \mathbf{x}_{Ant} , and \mathbf{x}_{GPS} are, respectively, the error vectors of the inertial navigation solution, the accelerometer measurement error, the gyro measurement error, the gravity anomaly and deflections, the antenna lever arm errors, and the GPS ionospheric errors; \mathbf{w}_{Nav} , \mathbf{w}_{Acc} , \mathbf{w}_{Gyro} , \mathbf{w}_{Grav} , and \mathbf{w}_{GPS} are all zero-mean Gaussian white noise vectors. More detailed expressions of the matrices F_{ij} ($j=1,2,3,4$) and F_{22} are provided in Appendix A.

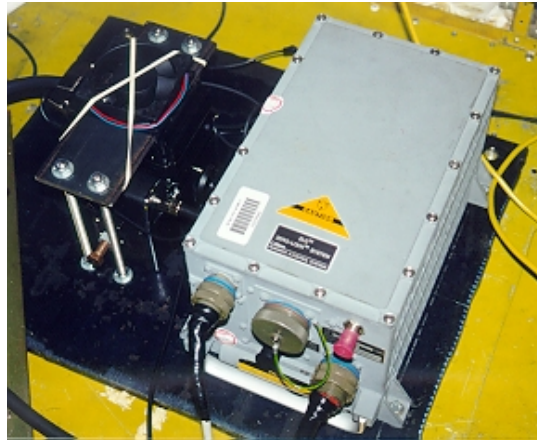


Figure 1. AIMS™ hardware configuration – INS and digital camera mount.

GRAVITY ERRORS IN INERTIAL NAVIGATION

Inertial navigation is based on Newton's second law of motion defined in the inertial (non-

$$\bar{\mathbf{r}} = \bar{\mathbf{a}} + \bar{\mathbf{g}} \quad (1)$$

rotating) frame. Thus, the basic mathematical model is expressed as the following system of

$$\bar{\mathbf{g}} = \bar{\mathbf{g}}_m + \Delta\bar{\mathbf{g}} \quad \text{and} \quad \Delta\bar{\mathbf{g}} = \begin{bmatrix} -\mathbf{g}_o\xi \\ -\mathbf{g}_o\eta \\ \Delta\mathbf{g} \end{bmatrix} \quad (2)$$

second order differential equations:

Where:

and $\bar{\mathbf{r}}$ is the total acceleration vector, $\bar{\mathbf{a}}$ is the acceleration sensed by the accelerometer, $\bar{\mathbf{g}}$ is the total gravitational acceleration vector, $\bar{\mathbf{g}}_m$ is the gravity model, $\Delta\bar{\mathbf{g}}$ is the difference between the actual gravity and the gravity model used, \mathbf{g}_o is the nominal value of gravity, ξ and η are vertical deflections of the vertical, and $\Delta\mathbf{g}$ is the gravity anomaly. Since the accelerometer triad

measures the difference between kinematic inertial acceleration and mass gravitation, errors in the measurements are affected by errors in knowledge of the gravity, leading ultimately to positioning errors. The uncertainty in gravity (deflections of the vertical and the gravity anomaly) is defined as the difference between the actual gravity and the gravity model implemented in the inertial navigation algorithm. Deflections of the vertical and the gravity anomaly contain the information mostly in the medium- to short-frequency range whereas the model usually represents the long wavelength part of the spectrum.

Different models, ranging from the normal gravity to high order spherical harmonic expansion, can be used to approximate the Earth's gravity field. The normal gravity model approximates the Earth's gravitation with an accuracy of 1 part in 10^4 , whereas detailed global gravitational models are good to 1 part in 10^5 [13]. Historically, normal gravity was satisfactory for free inertial navigation, but today's high-accuracy requirements for GPS-aided inertial systems bring even more demands for knowledge of the Earth's gravity field. During GPS outages, the quality of free-inertial navigation with the high- to medium-accuracy INS currently may well depend on the knowledge of the local gravity field. The gravity anomaly and deflection maps given on dense grids, based on gravimetric surveys, are becoming of more importance to applications that require precise navigation.

Errors in inertial navigation can be divided into two major groups – system related errors, and modeling errors. Measurement noise, calibration and alignment errors comprise the first group, whereas the second group contains approximation, linearization and lumping errors [2]. The uncertainties in the gravity vector fall in the second category, and are an important error source

for high-quality inertial navigation systems, especially during long missions, where the gravity errors tend to build up. The uncertainties in knowledge of the gravity field produce errors that cannot be eliminated by pure inertial system. In the aided navigation systems, however, sensor errors and the errors caused by gravity can be bounded. For example, an optimal combination of the inertial sensor with GPS allows continuous estimation of the errors in the inertial sensors and the gravity model, which can be fed back to the navigation algorithm, leading to a precise inertial navigation solution. Subsequently, an error-calibrated inertial system can be used for navigation during the GPS outages, and fills in between the GPS discrete trajectory estimates. A detailed expression of the INS system error model depends on the type of mathematical equations chosen for describing the gyro and accelerometer measurement errors, as well as for the gravity anomaly and deflections. Clearly, the filter design object is to achieve the desired modeling accuracy without unnecessarily increasing the complexity of the models and, thereby, the filter [11].

A vast array of literature exists discussing the effects of gravity uncertainties on inertial navigation, and stochastic gravity modeling. For a more detail discussion, and closed expressions for the various covariance models of anomalous gravity and deflections, the reader is referred to [19, 2, 14, 15, 23, 5, 6, 12, 13]. It is worth mentioning, however, that generally all the authors agree that the Gauss-Markov process can be used as the stochastic representation of the anomalous gravity field in the state vector estimation process. This implies that, by definition, the anomalous gravity field is stationary and its probability density is Gaussian. Medium-order (second to fourth) Gauss-Markov processes are considered as self-consistent in representing the anomalous gravity field, and therefore better serve the purpose than the first order process. Gauss-Markov models for the gravity field are, in general, designed to reflect the omission of the

long-wavelength component in the estimation process, and thus assume that the compensation models (or basic approximation) used are significantly higher than the normal gravity model. This implies that the unmodeled effects become more and more local in character.

In general, the higher the order of the spherical harmonic expansion used for computing the gravity intensity for the vertical axis in the navigation algorithm, the better the accuracy of the vertical velocity and altitude determination. Subsequently, since the velocity error couples from the vertical to horizontal axes (and vice versa) through the error in the Coriolis term, these effects are reduced as the velocity error is reduced due to less error from the gravity anomaly vector. Moreover, when the deflections of the vertical are compensated, there is less tilt error, and consequently, less coupling of the horizontal accelerations into the vertical axis. Thus, it can be expected that (high-accuracy) deflection of the vertical compensation should improve not only the positioning accuracy, but also the attitude determination of the platform. This can be verified by close examination of the dynamics matrix of the system, which shows the interrelation among the estimated errors. The errors in deflections of the vertical enter directly into the horizontal velocity errors in linear combination with the attitude errors. This, generally speaking, complicates full separation in the estimation procedure. Consequently, if one of the components, in this case DOV, becomes (partially) known, an improvement in estimation of the attitude should ultimately be achieved.

The following sections present the NIMA deflection of the vertical (DOV) data used in the airborne tests with the GPS/INS measurements and the system performance analysis with and without the partial deflection compensation.

NIMA DOV: PRODUCT DESCRIPTION

In the tests presented here, the unclassified NIMA Standard Inertial Navigation Product (INP) was used over the designated test areas. INP is a three-dimensional, gridded database of deflections of the vertical and their errors at 2'×2' separation ranging from 0 ft to 90K ft above the geoid level. It was derived from 1'×1' free-air gravity anomalies, selected from a NIMA point gravity anomaly (PGA) files using the Variable Interval selection program. The accuracy of the gravity anomaly ranges between 1 and 5 mgal (5 mgal corresponds roughly to 1 arcsec in deflection accuracy). A short description of the INP development process is given below [Steven Kenyon, NIMA, personal communication]. The GRAVSOFTE software package as described in [30], was used for INP development purpose. The designated reference system is WGS 84.

As a first gravity reduction step, the EGM96 (360, 360) gravity model was used to remove the long-wavelength effects from the original point gravity data. Subsequently, the high frequency components were also removed using Residual Terrain Models (RTM), implementing a prism integration technique. NIMA's most detailed set of 1'×1' Digital Terrain Elevation Data (DTED), along with 5' and 30' mean elevations, were used in the RTM computations process. After the EGM96 and RTM reductions, the point gravity was gridded to a 2'×2' mesh, using a local least-squares collocation procedure. The next step was to derive a 2'×2' grid of elevations from the original 1'×1' DTED, and use them to downward continue the gravity anomalies to the surface of the geoid. A two-kilometer attenuation factor was used.

Two-dimensional FFT transform of Vening Meinesz formulas were then employed to calculate DOV from the reduced free-air gravity anomalies. The entire area of conterminous US (CONUS) was segmented into $10^{\circ} \times 10^{\circ}$ blocks with 3-degree overlap. Based on the local covariance modeling technique, developed by Forsberg [5], least-squares collocation was used to obtain the accuracy estimates for the DOV. First the empirical covariance models were developed; next the analytical models with proper variance and correlation length were fit. Subsequently, the DOV were upward continued to 10K, 20K, and 30K ft elevations. Subsequently, the DOV due to RTM and EGM96 (360, 360) were computed at 0K, 10K, 20K, and 30K, and restored to the final predictions.

The bilinear interpolation to the three-dimensional locations in space that uses two neighboring layers of the gridded DOV data was applied to provide the final deflections to the strapdown navigation algorithm. The platform position at discrete 1-second locations was passed to the interpolating algorithm, and the current deflections were used for the entire second, for the 64 Hz navigation solution. The quality of the DOV data provided for the tests presented here was at the level (1 sigma) of 0.5 arcsec [Steven Kenyon, NIMA, personal communication]. However, a somewhat conservative standard deviation of 1 arcsec was used in the data processing.

NUMERICAL RESULTS

Effects of DOV compensation on the positioning and attitude estimates

The model most commonly used for the effects of the anomalous gravity field in the state vector is the time correlated noise process, as mentioned in the previous sections. The second- to fourth-order Gauss-Markov process combined with the high-order reference field is recommended by

[15, 23, 12]. However, the first-order Gauss-Markov process is often used for its simplicity, and was also applied together with normal gravity as a basic gravity field approximation, in the data reduction for the tests presented in this section. It should be mentioned that the first order Gauss-Markov process, combined with normal gravity as a basic approximation, can understate the actual errors in the horizontal gravity components, primarily due to the fact that the very long wavelength cannot be estimated [12].

The test flights analyzed in this paper were conducted in 1997 and early 1998 with St. Louis-based Image America (formerly OMNI Solutions International Ltd) in the St. Louis area. A total of two missions comprising four test flights (see Table 3) were flown to evaluate the performance of the integrated positioning/orientation component. The data collected during these tests were processed with two different data reduction modes provided by the AIMS™ software — mode 1, where no prior knowledge of DOV was assumed, and mode 2, where the NIMA 2'×2' DOV data were used — with RMS (1 sigma) of 1 arcsec. The first-order Gauss-Markov process was used as a stochastic representation of the anomalous gravity field as indicated above (see Table 2).

Flight Number	Date	Altitude [m]	Speed [m/s]
1	4/23/98	4500	125
2	4/24/98	4800	120
3	3/6/97	4800	120
4	3/6/97	4800	125

Table 3. Test flight schedule.

The position and orientation estimates from both processing modes were compared, and typical results are presented in Figures 2-5 and Table 4. Figure 2 illustrates the attitude difference between the solutions, i.e., with and without DOV data, for the steady-state portion of test flight #2. The estimated attitude standard deviations (square roots of the diagonal terms of the filter covariance matrix) for the same steady-state portion of test flight 2, for DOV-compensated case are shown in Figures 3 and 4, whereas their counterparts from the DOV-uncompensated solution are shown in Figure 5. The comparison of Figures 3, 4, and 5 indicates improvement in the estimated standard deviations with respect to mode 1 by 1.5-2.5 arcsec. This represents the average gain due to the DOV compensation, and is observed at a similar level for all the analyzed test flights. In addition, some improvement in the order of 1 arcsec (average) for the heading standard deviation was observed. Generally, the DOV-compensated solution shows faster convergence and steadier spectrum of the standard deviation, as compared to the uncompensated mode. Table 4 presents the summary of the comparison between both processing modes for the test flights listed in Table 3. It shows that the RMS of the attitude differences ranges from 3 to 5.6 arcsec for pitch, and 3.1 to 17.2 for roll, with the largest differences reaching 14 and 21.4 arcsec, respectively.

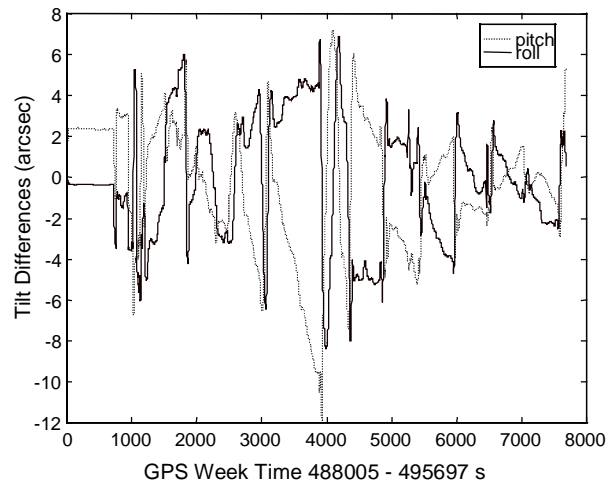


Figure 2. Differences in attitude between solutions with and without DOV compensation (flight 2).

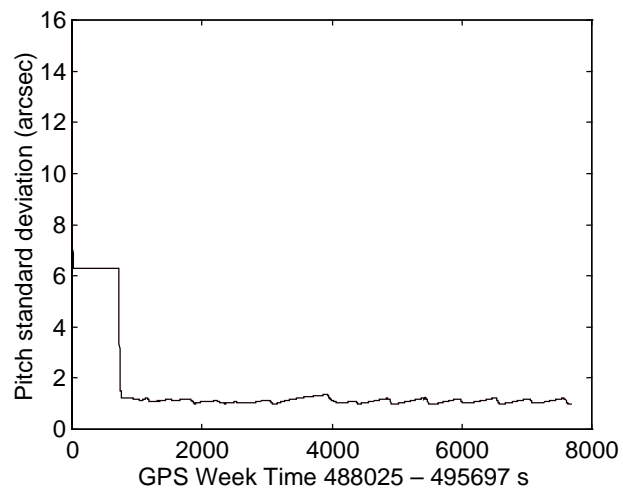


Figure 3. Pitch standard deviation (square roots of the diagonal terms of the filter covariance matrix) for solution with DOV compensation (flight 2).

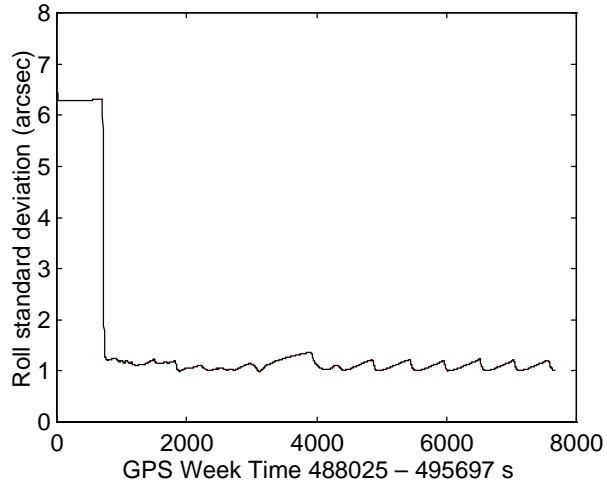


Figure 4. Roll standard deviation (square roots of the diagonal terms of the filter covariance matrix) for solution with DOV compensation (flight 2).

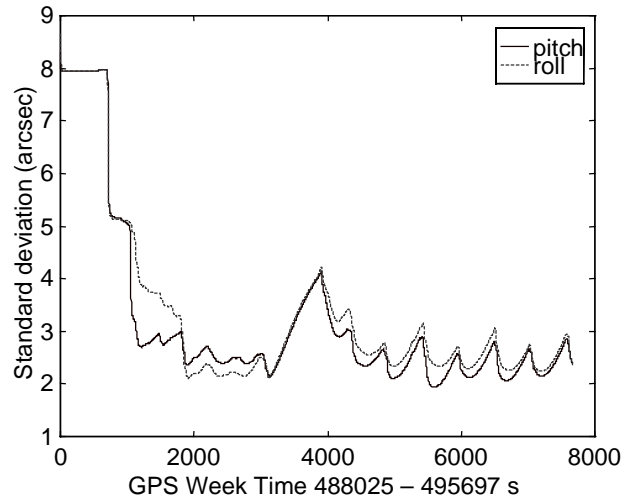


Figure 5. Attitude standard deviation (square roots of the diagonal terms of the filter covariance matrix) for solution without DOV compensation (flight 2).

Tilt	Flight #	RMS [arcsec]	Max [arcsec]	Mean [arcsec]
Pitch	1	3.9	10.9	1.7
	2	3.0	8.4	-0.1
	3	5.6	12.2	-1.6
	4	3.9	-14.0	-3.2
Roll	1	3.3	-11.1	-0.8
	2	3.1	11.1	-0.4
	3	4.0	12.1	2.7
	4	17.2	-21.4	-17.1

Table 4. Difference in attitude between solutions with and without DOV compensation.

Figures 6 and 7 illustrate the deflection of the vertical compensation used in the flight #2 data reduction process. It shows, that north-south DOV, changes between 1 and 5 arcsec for the entire flight duration. The east-west component is significantly smaller, ranging from 0.5 to -2.5 arcsec. The amount of compensation applied in mode 2 is reflected in the order of magnitude of the attitude differences between both solutions, as plotted in Figure 2.

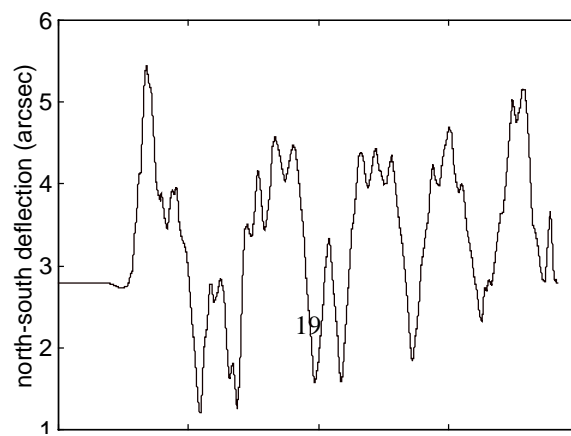


Figure 6. North-south deflection signature, flight #2.

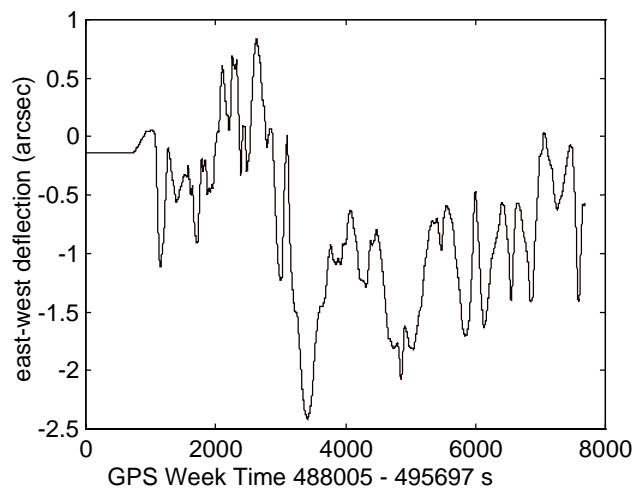


Figure 7. East-west deflection signature, flight #2.

One aspect worth analyzing is the behavior of the attitude standard deviations related to filter's covariance matrix, as a function of the flight trajectory. For example, the portion of the flight between epochs ~3000-4000 in Figures 3-5 corresponds to a longer (~ 90 km) straight portion of the trajectory, where no maneuvers were performed. It appears that for the solution without DOV compensation the attitude standard deviations show an increase from 2 to 4 arcsec, whereas in the DOV-compensated case they show a rather flat spectrum at ~1.5 arcsec level, with only very minor growth at the specified interval. The aircraft maneuvers following this part of the trajectory brought the mode 1 estimated errors in attitude down to the 3 arcsec level.

Another test performed with the results from both solutions (i.e., DOV-compensated and uncompensated) is illustrated in Figures 8-11. They show typical horizontal error growth and positional standard deviations during the outage of the GPS signal. In both cases, the filter was run for approximately 15 minutes to allow for error calibration, and then an intentional gap of 60 s was introduced to both solutions at epoch marked 60 in Figures 8-11. Resulting trajectories were compared to the reference truth based on DGPS/INS post-mission solution. The results from the DOV-compensated case show an improvement of about 50% in the error level of the north component, and some minor improvement in the east component (Figure 10), as compared to Figure 8, which illustrates the DOV-uncompensated results. The respective positional standard deviations (square roots of the diagonal terms of the filter covariance matrix) also show improvement of ~20%, as compared to the solution with no DOV compensation. Smaller improvement in the east component contrary to the north coordinate can be explained by smaller DOV signature observed in east-west direction of the analyzed flight. It can be observed from

Figure 8 that the average error growth rate is about 1.2 mm/s for the north, and 0.4 mm/s for the east component, for the first 60 s of GPS total loss of lock. These results indicate that most of the correlated IMU errors have been correctly estimated by the Kalman filter, and removed from the IMU measurements by the feedback update loop. Thus, the system is able to provide accurate velocity and position information even when GPS lock is lost for a short period of time. Moreover, an introduction of gravity compensation leads to further improvement, lowering the rate growth for the north component to 0.5 mm/s. A high quality of free inertial navigation during the GPS outages is very important for fast ambiguity recovery after tracking is reestablished. It supports the GPS cycle-slip correction, and makes fast and robust On-The-Fly (OTF) ambiguity resolution possible. INS error growth in AIMS™ is below 10 cm for the horizontal components, even for solution without DOV compensation, and below 20 cm in the vertical direction (not shown here), after a 60-second loss of GPS lock, which still enables instantaneous ambiguity recovery after the GPS signal is recovered (for details see Grejner-Brzezinska et al., 1998].

In order to test the influence of DOV compensation on the positional error for the extended period of the free navigation mode, the Kalman filter was calibrated for about 1000 s, and subsequently the GPS signal was intentionally cut off for 3000 s. This was repeated for two independent solutions – with and without DOV compensation. The resulting trajectories were again compared to the GPS/INS post-processed truth trajectory, and the differences in the north coordinate are plotted in Figure 12. It can be observed that the DOV-compensated solution shows positional error smaller by 20-50 m, as compared to DOV- uncompensated solution, depending on the error in compensation itself and the total duration of the free navigation mode.

The positional errors due to gravity in the DOV-compensated case result from the finite grid resolution (2'), which might not capture the shorter wavelength signature, and the accuracy of DOV itself (assumed at 1 arcsec). It should also be mentioned that the east component (not shown here) presents similar behavior.

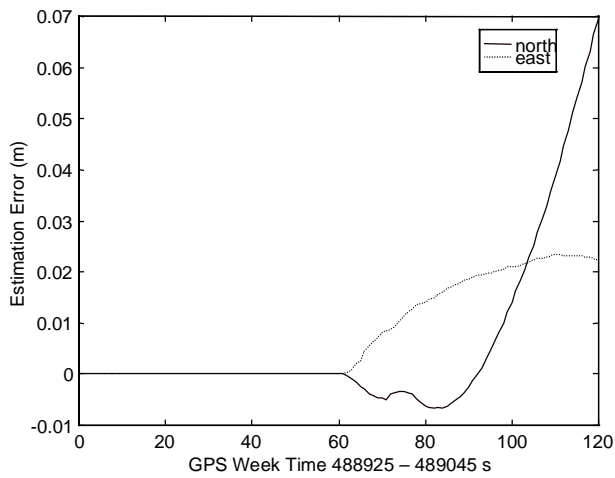


Figure 8. Horizontal error growth during GPS outage introduced at epoch 60: solutions without DOV compensation.

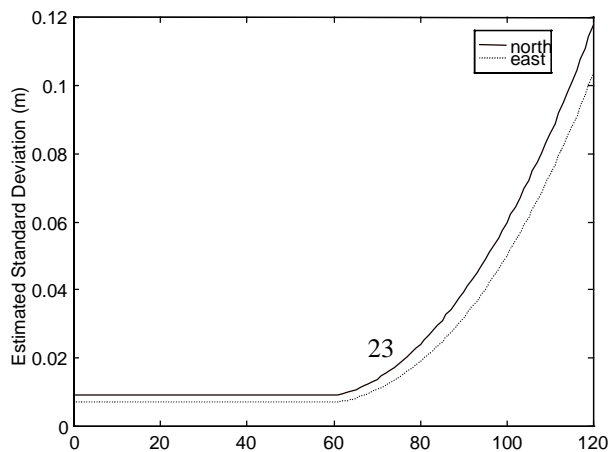


Figure 9. Estimated standard deviations (square roots of the diagonal terms of the filter covariance matrix) of the horizontal positioning during GPS outage introduced at epoch 60: solution without DOV compensation.

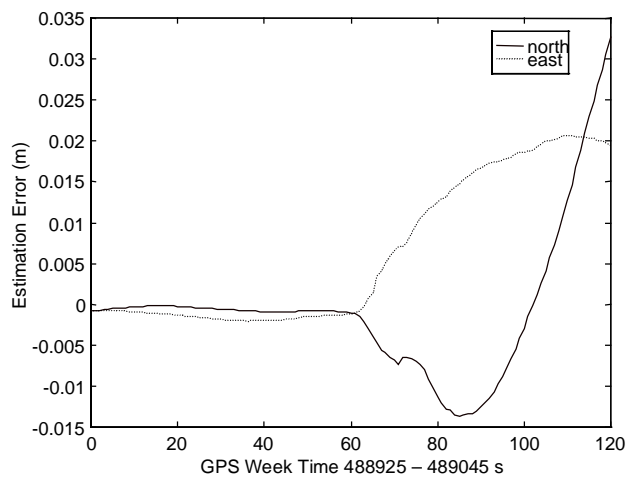


Figure 10. Horizontal error growth during GPS outage introduced at epoch 60: solution with DOV compensation.

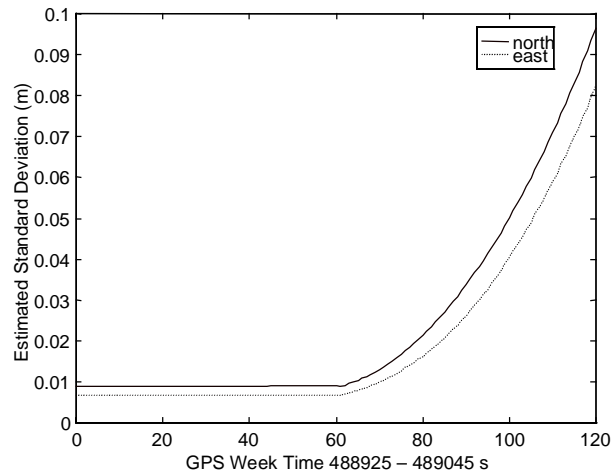


Figure 11. Estimated standard deviations (square roots of the diagonal terms of the filter covariance matrix) of the horizontal positioning during GPS outage introduced at epoch 60: solution with DOV compensation.

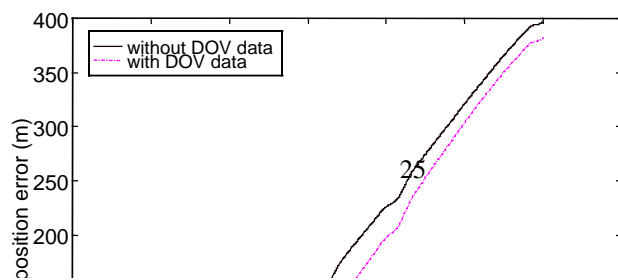


Figure 12. North coordinate error growth, free navigation mode with DOV compensation.

Third order Gauss-Markov model for gravity anomaly and vertical deflections

As discussed in the previous sections, the first order Gauss-Markov process is not considered an optimal stochastic representation for the anomalous gravity field, especially if the normal gravity is used as a basic approximation for the gravity signature in the navigation algorithm. In order to test the effects of different stochastic models for gravity anomaly and deflections on the filtering results, a third-order Gauss-Markov model, which properly reflects the strong attenuation of gravity signal with attitude, was initially implemented (1 sigma for deflections = 25 mgal, 1 sigma for gravity anomaly = 35 mgal, $T = 20$ nmi for all three components). The positioning results from a test flight over the Madison, OH test range, obtained with the third-order Gauss-Markov model for gravity were compared to the corresponding first-order Gauss-Markov processing results, as shown in Figure 13. The difference in horizontal coordinates ranges between 2 and 6 cm, whereas vertical components differ by 10 cm at most, being at the level of

2-3 cm for most of the flight. The results presented here are preliminary; more tests have to be conducted towards estimating the best correlation distances for gravity anomaly and deflections.

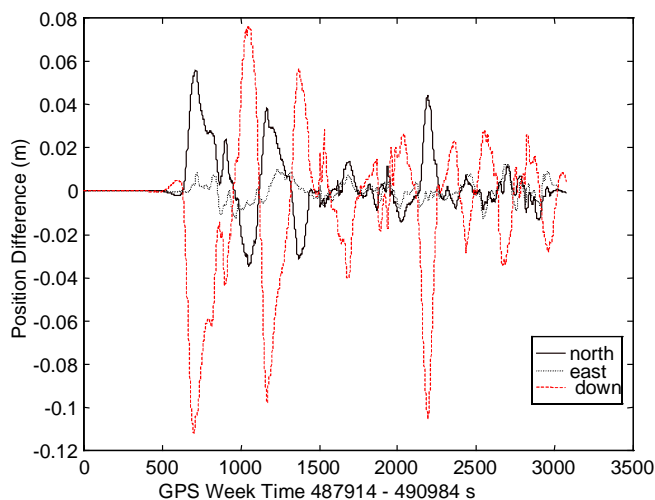


Figure 13. Positioning results difference between solutions with 1st and 3rd order Gauss-Markov models for gravity.

CONCLUSIONS

The major objective of this paper was to test the feasibility of attitude estimation improvement by using high-accuracy DOV information in the integrated GPS/INS navigation system. The covariance analysis results indicate that the estimability of the attitude components improves by adding partially compensated (1 arcsec RMS) gravity information. The Kalman filter converges faster and the standard deviation spectrum is less sensitive to the lack of maneuvers, which is normally observed during the straight portions of the flight. Free inertial navigation during the

GPS outages in DOV-compensated mode shows slower error accumulation, especially in the horizontal components, as compared to the DOV-uncompensated solution. However, these results are preliminary and some improvements are needed, especially in the stochastic modeling of the gravity anomaly vector, as indicated in the previous section.

ACKNOWLEDGEMENTS

The AIMS™ project is supported by the NASA Stennis Space Center, MS, Commercial Remote Sensing Program grant #NAG13-42, and a grant from Litton Systems, Inc. Special thanks go to Richard Salman and Steven Kenyon from NIMA, St. Louis office, for providing the gravity data for the test flights analyzed here.

REFERENCES

1. Abdullah, Q., *Evaluation of GPS-Inertial Navigation System for Airborne Photogrammetry*, presented at 1997 ACSM/ASPRS Annual Convention and Exposition, April 7-10, 1997, Seattle, WA.
2. Britting, K. R., *Inertial Navigation Systems Analysis*, New York: Wiley-Interscience, 1971.
3. Brozena, J. M., Peters, M. F., *The Greenland Aerogeophysics Project: Year 1*, presented at ION 48th Annual Meeting, 1992.
4. Da, R., *Investigation of Low-Cost and High-Accuracy GPS/IMU System*, Proceedings of ION National Technical Meeting, January 14-16, 1997, Santa Monica, pp. 955-963.

5. Forsberg, R., *A New Covariance Model for Inertial Gravimetry and Gradiometry*, JOURNAL OF GEOPHYSICAL RESEARCH, Vol. 92 (B2), 1987, pp. 1305-1310.
6. Gleason, D. M., *Extracting Gravity Vectors from the Integration of Global Positioning System and Inertial Navigation System Data*, JOURNAL OF GEOPHYSICAL RESEARCH, Vol. 97(B6), 1992, pp. 8853-8864.
7. Grejner-Brzezinska, D. A., *Airborne Integrated Mapping System: Positioning Component*, Proceedings of 53rd ION Annual Meeting, June 30-July 2, 1997, Albuquerque, NM, pp. 225-235.
8. Grejner-Brzezinska D. A., Phuyal B. P., *Positioning Accuracy of the Airborne Integrated Mapping System*, Proceedings of ION Technical Meeting, January 21-23, 1998, Long Beach, CA, pp. 713-721.
9. Grejner-Brzezinska D. A., Da, R., Toth C., *High-Accuracy GPS/INS Integration for The Airborne Large Scale Mapping*, accepted for JOURNAL OF GEODESY, 1998.
10. Hagstrom, T., Miller, M., Atkinson, D., Davis, R., *High Accuracy Gravity Disturbance Surveys Using an Astro Inertial Navigation System with Differential GPS*, Proceedings of ION 53rd Annual Meeting, June 30-July 2, 1997, Albuquerque, NM, pp. 237-243.
11. Huddle, J. R., *Inertial Navigation System Error Model Considerations in Kalman Filter Applications*, CONTROL AND DYNAMIC SYSTEMS (ed. C. T. Leondes), 1983, Vol. 20, No.2, pp. 294-340.
12. Jekeli, C., *Airborne Vector Gravimetry Using Precise, Position-Aided Inertial Measurement Units*, BULLETIN GEODESIQUE, 1994, Vol. 69, pp.1-11.
13. Jekeli, C., *The Effect of Earth's Gravity on Precise Short-Term, 3-D Free-Inertial Navigation*, NAVIGATION, 1997, Vol. 44, No. 3, pp. 347-357.

14. Jordan, S. K., *Self-consistent Statistical Models for the Gravity Anomaly, Vertical Deflections and Undulations of the Geoid*, JOURNAL OF GEOPHYSICAL RESEARCH, 1972, Vol. 77.
15. Jordan, S. K., *Effects of Geodetic Uncertainties on a Damped Inertial Navigation System*, IEEE TRANSACTIONS ON AEROSPACE AND ELECTRONIC SYSTEMS, 1973, Vol. AES-9, No. 5, pp. 741-752.
16. Jordan, S. K., Center, J. L., *Establishing Requirements for Gravity Surveys for Very Accurate Inertial Navigation*, NAVIGATION, 1986, Vol. 33, No. 2, pp. 90-108.
17. Kerr III, T., *Use of GPS/INS in the Design of Airborne Multisensor Data Collection Mission (for Tuning NN-based ATR Algorithms)*, Proceedings of ION GPS, September 17-20, 1994, Salt Lake City, Utah, pp.1173-1188.
18. Lachapelle, G., Lu, G., and Loncarevic, B., *Precise Shipborne Attitude Determination Using Wide Antenna Spacing*, Proceedings KIS94, 1994.
19. Levine, S. A., Gelb, A., *Effect of Deflections of the vertical on the Performance of a Terrestrial Navigation System*, JOURNAL OF SPACECRAFT AND ROCKETS, 1968, Vol. 6, pp. 97-984.
20. Lithopoulos, E., Reid, B., Scherzinger, B., *The Position and Orientation System (POS) for Survey Applications*, International Archives of Photogrammetry and Remote Sensing, ISPRS Comm. III, 1996, Vol. XXXI, part B3, pp. 467-471.
21. Litton Systems, Inc., *LN-100G EGI Description*, Litton Systems, Inc., September 1994.
22. Scaloud, J., Cramer, M., Schwarz, K.P., *Exterior Orientation by Direct Measurement of Camera Position and Attitude*, International Archives of Photogrammetry and Remote Sensing, 1996, Vol. XXXI, Part B3, pp. 125-130.

23. Schwarz, K. P., *Gravity Induced Position Errors in Airborne Inertial Navigation*, Report No. 326, Department of Geodetic Science and Surveying, The Ohio State University, 1981.
24. Schwarz, K. P., *Kinematic Modeling – Progress and Problems*, Kinematic Systems in Geodesy, Surveying and Remote Sensing (ed. K.P. Schwarz and G. Lachapelle), Springer-Verlag, 1990, pp. 3-16.
25. Schwarz, K. P., *INS/GPS as a Georeferencing Tool for Multi-Sensor Systems*, presented at the Mobile Mapping Symposium, May 24-26, 1995, Columbus, OH.
26. Schwarz, K. P., Colombo, O., Hein, G., Knickmeyer, E. T., *Requirements for Airborne Vector Gravimetry*, Proceedings of IAG Symp. From Mars to Greenland: Charting Gravity with Space and Airborne Instruments, General Assembly of the IUGG, Vienna 1991, Springer Verlag, New York, 1992, pp. 273-283.
27. Schwarz, K. P., Wei, M., *Aided Versus Embedded A Comparison of Two Approaches to GPS/INS Integration*, Proceedings of IEEE Position Location and Navigation Symposium, April 11-15, 1994, Las Vegas, NE, pp. 314-321.
28. Toth, C., *Direct Sensor Platform Orientation: Airborne Integrated Mapping System (AIMS)*, ISPRS Comm. III, 1997, Vol. XXXII, part 3-2W3, pp. 148-155.
29. Toth, C.K., Grejner-Brzezinska, D.A., *Performance Analysis of the Airborne Integrated Mapping System (AIMS™)*, Proceedings of ISPRS Comm. II, Cambridge, UK, July 13-17, 1998, pp. 320-326.
30. Tscherning, C.C., P.Knudsen and R.Forsberg, *Description of the GRAVSOF T package*, Geophysical Institute, University of Copenhagen, Technical Report, 1994.

31. Wang, J., *Gravity Recovery by LN-93 Strapdown Airborne Gravity System – A Comparison of Different Gravimetry Approaches Based on Simulation*, Report No. 439, Geodetic Science and Surveying, The Ohio State University, 1997.
32. Ward, L., Axelrad, P., *A Combined Filter for GPS-based Attitude and Baseline Determination*, *NAVIGATION*, 1997, Vol. 44, pp.195-213.

Appendix A: System Dynamics

Detailed expression for sub-matrices F_{1j} ($j=1,2,3,4$) and F_{22} of the dynamics matrix F from Equation (1):

$$F_{11} = \begin{bmatrix} 0 & -\mathcal{L} & \mathcal{E} & 1 & 0 & 0 & 0 & 0 & 0 \\ \mathcal{L} & 0 & \mathcal{E} & 0 & 1 & 0 & 0 & 0 & 0 \\ -\mathcal{E} & -\mathcal{L} & 0 & 0 & 0 & 1 & 0 & 0 & 0 \\ -\frac{g}{R_e} & 0 & 0 & 0 & -(2\omega_{ie} + \mathcal{L})sL & \mathcal{E} & 0 & -f_D & f_E \\ 0 & -\frac{g}{R_e} & 0 & (2\omega_{ie} + \mathcal{L})sL & 0 & (2\omega_{ie} + \mathcal{L})cL & f_D & 0 & -f_N \\ 0 & 0 & \frac{2g}{R_e} & -\mathcal{E} & -(2\omega_{ie} + \mathcal{L})cL & 0 & -f_E & f_N & 0 \\ 0 & 0 & 0 & 0 & 0 & 0 & 0 & -(\omega_{ie} + \mathcal{L})sL & \mathcal{E} \\ 0 & 0 & 0 & 0 & 0 & 0 & (\omega_{ie} + \mathcal{L})sL & 0 & -(\omega_{ie} + \mathcal{L})sL \\ 0 & 0 & 0 & 0 & 0 & 0 & -\mathcal{E} & (\omega_{ie} + \mathcal{L})sL & 0 \end{bmatrix} \quad (A1)$$

where

$$(sL = \sin(L), cL = \cos(L))$$

$$F_{12} = I(3 \times 3) \quad (A2)$$

$$F_{13} = \begin{bmatrix} 0(3 \times 3) & 0(3 \times 3) \\ C_b^n & C_b^n \begin{bmatrix} f_x & 0 & 0 \\ 0 & f_y & 0 \\ 0 & 0 & f_z \end{bmatrix} \\ 0(3 \times 3) & 0(3 \times 3) \end{bmatrix} \quad (A3)$$

$$F_{14} = \begin{bmatrix} 0(6 \times 3) & 0(6 \times 3) \\ -C_b^n & -C_b^n \begin{bmatrix} \omega_x & 0 & 0 \\ 0 & \omega_y & 0 \\ 0 & 0 & \omega_z \end{bmatrix} \end{bmatrix} \quad (A4)$$

$$F_{22} = \text{diag}[-\tau_{gN} \quad -\tau_{gE} \quad -\tau_{gD}] \quad (A5)$$

In the equations above C_b^n is the direction cosine matrix from body-fixed frame (b -frame) to navigation frame (n -frame), ω_{ie} is the Earth's rotation rate, L is the geodetic latitude, and λ is the geodetic longitude, g is the gravity constant, (f_x, f_y, f_z) is the accelerometer sensed specific force vector defined in the b -frame, (f_N, f_E, f_D) is the same specific force vector coordinatized in the b -frame, $(\omega_x, \omega_y, \omega_z)$ is the gyro sensed vehicle rotation rate vector. R_e equals the Earth radius plus vehicle altitude, and τ_g is the time constant for the Markov processes of gravity uncertainties.